ACS Photonics

pubs.acs.org/journal/apchd5

Article

Ultraviolet Metalens Based on Nonlinear Wavefront Manipulation of Lithium Niobate Metasurfaces

Yunan Liu, Bo Wang,* Leyong Hu, Xu Ji, Tingyue Zhu, Ruhao Pan,* Haifang Yang, Changzhi Gu, and Junjie Li*

Cite This: https://doi.org/10.1021/acsphotonics.4c02259

Read Online

ACCESS | Metrics & More | Article Recommendations | Supporting Information

ABSTRACT: Nonlinear metalens has revolutionized the generation and focusing of nonlinear harmonic waves, significantly enhancing the performance of nonlinear frequency converters and expanding the applications of metalens from linear optics to nonlinear optics. However, current nonlinear metalens are typically constructed using low-nonlinear-susceptibility materials, impeding further advancements in the field. Here, we have developed a nonlinear metalens utilizing crystallized lithium niobate (LN), a material with a large second-order susceptibility and a broad transparent window. The meta-atoms of the LN metalens consist of elliptical nanoholes, fabricated by using a self-developed multiatmosphere cooperative etching technique. With a diameter of 200 μm, our fabricated metalens can focus the second harmonic wave at 390 nm to a 0.7-μm-wide spot with a focus length of 100 μm, resulting in a numerical aperture of 0.7. The peak intensity of the focus plane is enhanced by 40 times. Our LN metalens has potential applications in versatile nonlinear meta-optic devices for highly efficient frequency converting, high-resolution imaging, and bright entangled photopairs.

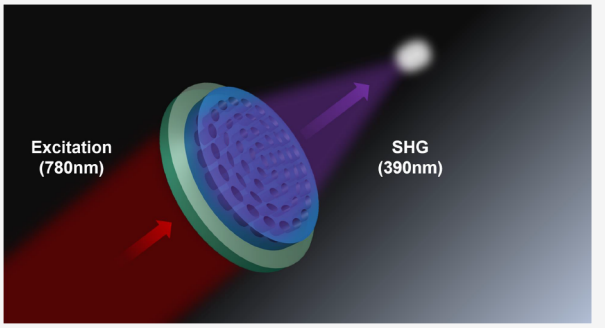

KEYWORDS: *lithium niobate, metasurfaces, second harmonic generation, metalens, ultraviolet focus*

INTRODUCTION

In recent years, metasurfaces have garnered significant scientific and technological attention due to their ability to modulate amplitude, phase, and polarization in a compact space using a spatially engineered planar array of subwavelength artificial resonators.[1−6] These ultrathin structures have the powerful ability to shape and control complex optical wavefronts, leading to the emergence of flat metalens. Metalens have already brought evolutionary technological breakthroughs to traditional optical lens systems and imaging[7−11] and have enormous potential applications in high-resolution imaging,[12,13] virtual reality/augmented reality,[14,15] depth sensing,[16] color routing,[17,18] optical zoom,[19] and polarization detection.[20] The most critical aspect of designing metalens is creating a spatially varying phase profile, which can be achieved through the resonant phase,[21] the propagation phase,[22] and the Pancharatnam−Berry phase.[23,24] While early research on metalens relied on linear optical interactions to generate local phase gradients, pioneer works have introduced nonlinear optical effects in metasurfaces,[25] opening up new possibilities such as all-optical mode control and generating nonlinear optical vortices, especially generating entangled photon pairs. Also, nonlinear metalens have been developed based on these nonlinear metasurfaces, and they permit focusing light at new frequencies that are difficult to reach with linear metasurfaces, such as deep ultraviolet light.[26,27] Additionally, in strong-field laser techniques, two-color laser fields are widely used to manipulate light−matter interactions, which usually require the simultaneous generation and focusing of second harmonics. Nonlinear metalens, therefore, have great potential applications in strong laser physics.

Second harmonic generation (SHG) is one of the most important nonlinear optical processes. Nonlinear metalens based on SHG have been reported.[26] Early demonstrations used metal nanostructures with 3-fold rotation symmetry, whose nonlinear PB phase is engineered to generate spherical phase distributions.[28] However, metals usually have a vanished intrinsic second-order susceptibility. Moreover, inherent ohmic loss and a low laser-damaged threshold of metals impede the efficiency of nonlinear frequency conversion. Very recently, ZnO, an all-dielectric material that is a counterpart of metal nanoresonators, was used to construct nonlinear metalens for generating and focusing violet light.[26] However, the $\chi^{(2)}$ of ZnO is ∼0.2 pm/V, which is weaker than those of most conventional $\chi^{(2)}$ materials. Some other $\chi^{(2)}$ materials with

Received: November 14, 2024
Revised: March 11, 2025
Accepted: March 13, 2025

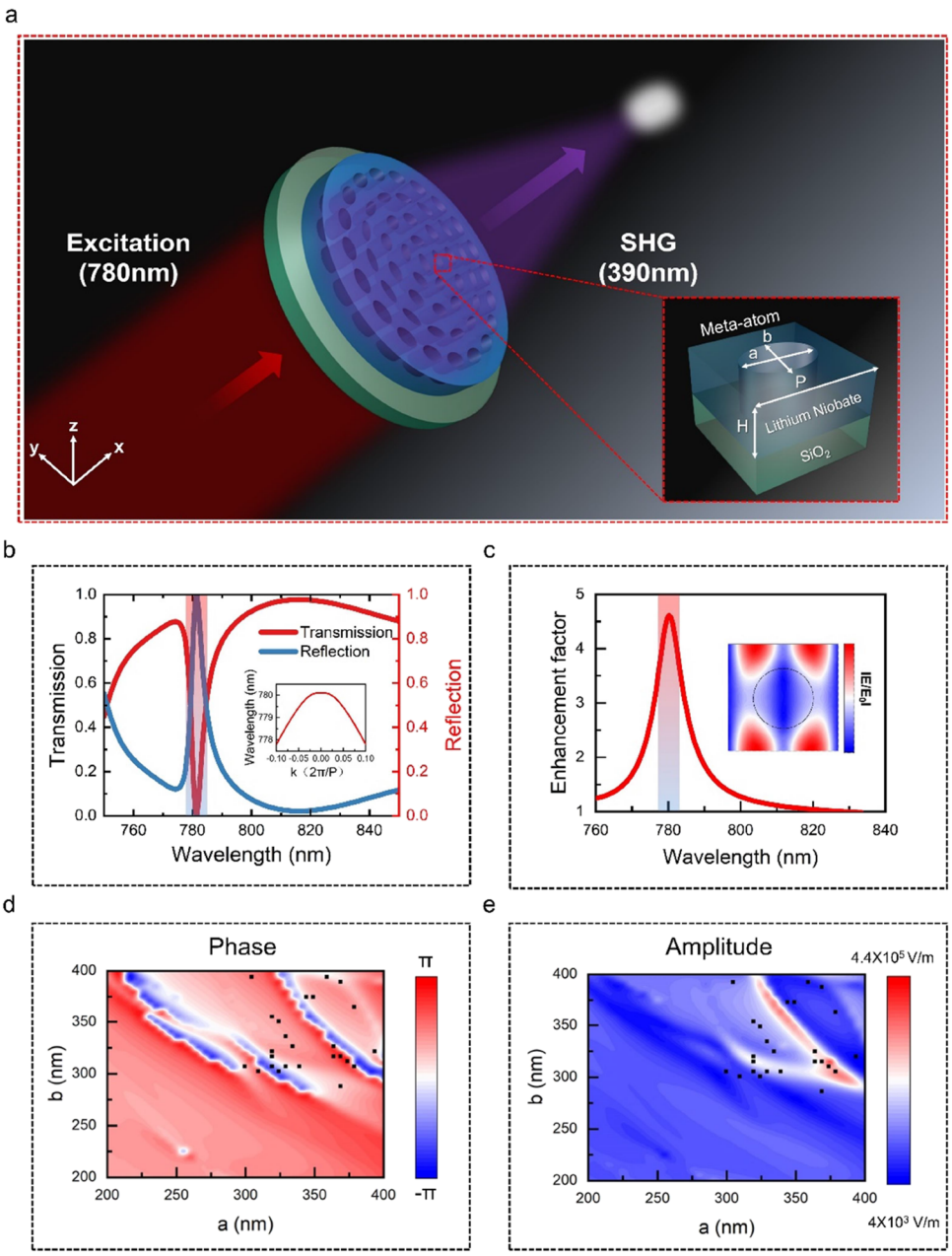

Figure 1. LN ultraviolet nonlinear metalens design. (a) Idealized schematic. Inset: Geometric parameters of the meta-atom: thickness: H = 300 nm; period: P = 480 nm. (b) Simulated transmission and reflection spectra. Inset: Calculated band diagram of the meta-atoms. The resonance wavelength is located at 780 nm. (c) Calculated average enhancement factor of the electric field. Inset: Near-field distributions of the local electric field ($|E/E_0|$) in the y−z plane. (d,e) Phase (d) and amplitude (e) of the second harmonic waves varying with the major and minor axis lengths of the ellipses.

relatively large $\chi^{(2)}$, such as GaAs and InP, are opaque in the visible spectrum, limiting their utility in metalens design.

To address these limitations, attention has shifted toward the lithium niobate (LN) material, often labeled as the "silicon of photonics".[29] LN offers exceptional properties such as remarkable electro-optic performance, superior optical birefringence, thermal characteristics, and, most notably, minimal loss across a wide bandwidth and exceptional second-order nonlinear performance.[30−34] These attributes render it an ideal candidate for nonlinear metalens applications. Nonetheless, the stable crystal structure of LN presents significant challenges in achieving precise nanostructuring.[33] At present, LN nanostructures are mainly employed for enhancing SHG,[34−37] electro-optics,[38,39] quantum optics,[40,41] and on-chip integration[42−46]; however, no attempts have been made to develop a nonlinear nanoscale metalens using LN due to the limitations of LN nanofabrication technology.

In this work, we report the conversion of near-infrared light (780 nm) to ultraviolet light (390 nm) while simultaneously focusing the ultraviolet light using an LN metalens. This achievement is facilitated by our self-developed multiatmosphere cooperative etching technique for LN materials, enabling the fabrication of LN nanostructures with high precision. Our metalens exhibits a high numerical aperture of 0.7 and enhances SHG by nearly 40 times at the focal point. The measured full width at half-maximum (fwhm) of the focal

https://doi.org/10.1021/acsphotonics.4c02259
ACS Photonics XXXX, XXX, XXX−XXX

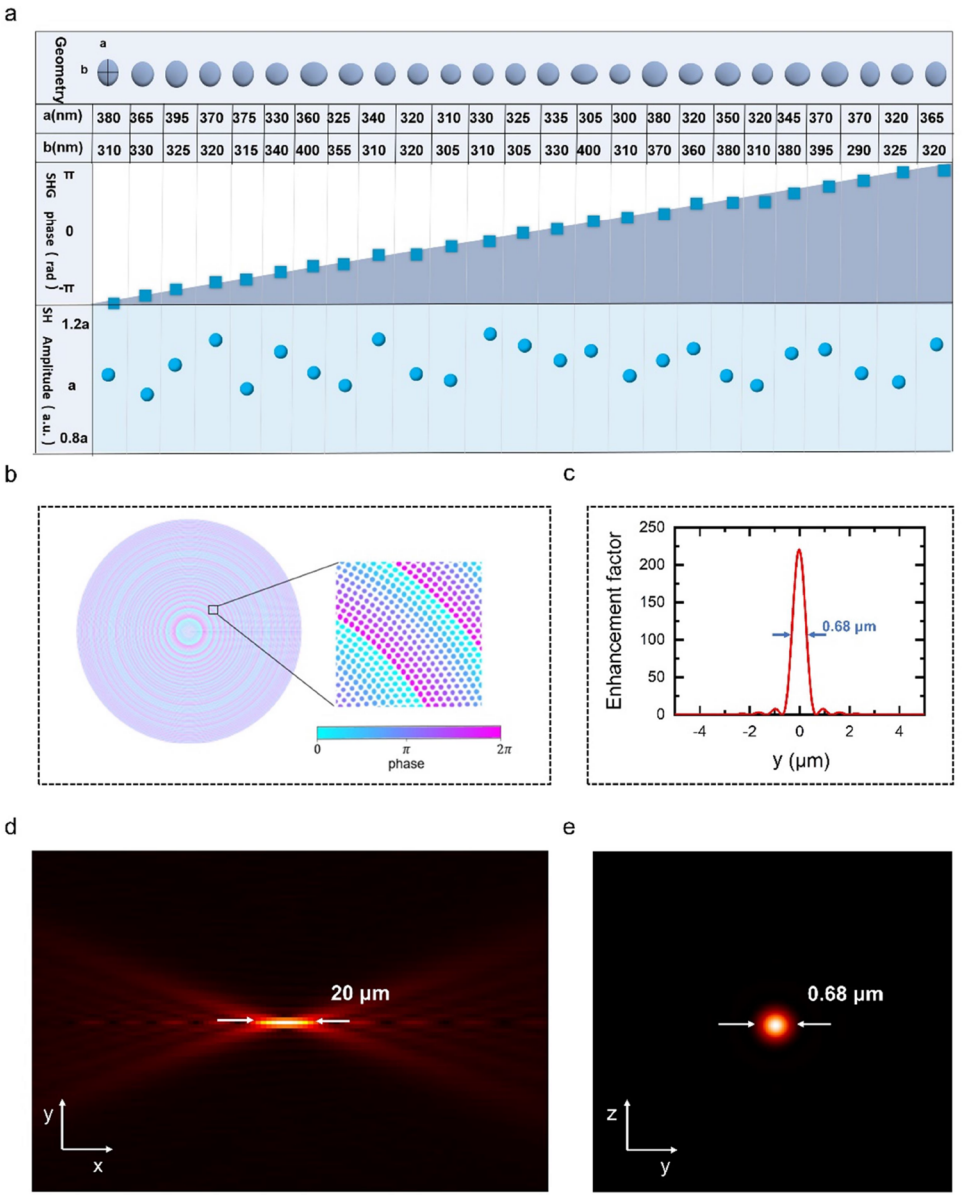

Figure 2. Simulation results of the LN metalens. (a) Meta-atom structures with elliptical holes of different sizes (geometry, second harmonic phase, and second harmonic amplitude). (b) Layout of the nonlinear metalens. A color code is imposed on the meta-atoms with different sizes to illustrate the phase profile encoded on the metalens. An enlarged image of the phase profile is shown as the inset. (c) Simulation of the enhancement factor in the y-direction. (d,e) Simulation of the focusing effect of the metalens in the $x-y$ plane (d) and $y-z$ plane (e).

spot is 0.7 μm, approaching the diffraction limit. This work not only addresses a significant gap in the field of nonlinear metalens based on LN but also provides crucial technical support for the integration of LN materials in micro- and nanophotonics, nonlinear photonics, and on-chip integration.

RESULTS AND DISCUSSION

Nonlinear Metalens Design. Figure 1a shows a schematic of the designed nonlinear LN metalens. The building blocks are elliptical nanoholes (see the inset of Figure 1a). They are arranged carefully so that the generated second harmonic waves can be focused due to the spatially varying phase profile, as will be shown below. Since the LN material has intrinsic anisotropy, the nonlinear geometric phase resulting from the rotation symmetry of the LN structure will be very complicated. Therefore, we consider the resonant phase, where the phase of SHG is continuously controlled near a resonance associated with the fundamental waves. We chose circular nanoholes as initial meta-atoms. A periodical array of LN nanoholes supports guided resonant modes (see the energy band in the inset of Figure 1b and simulation details in Supplementary Note I). At the Γ point of the Brillouin zone, the resonant wavelength is 780 nm, and the Q factor is ∼70. Figure 1b shows the transmission and reflection spectra, where the resonant structures around 780 nm are obvious. The guided mode resonances can enhance the local field inside the high-index region, as shown in the inset of Figure 1c, which is commonly used to improve the nonlinear frequency conversion efficiency. Figure 1c shows the calculated average field enhancement factor, which is defined as $\int_{LN}|E/E_0|dV/V$, where E is the local electric field, E_0 is the incident electric field, and V is the volume of the LN region. The field enhancement factor is ∼4.5 at 780 nm. The simulated SHG efficiency of the LN nanohole structure is ∼10 times higher

https://doi.org/10.1021/acsphotonics.4c02259
ACS Photonics XXXX, XXX, XXX−XXX

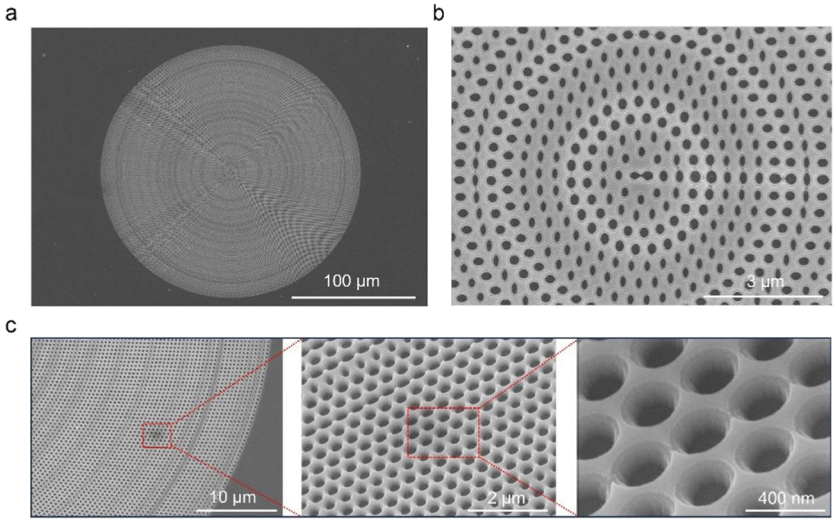

Figure 3. SEM images of the metalens (52° tilted and vertical view). (a) Complete metalens. (b) Pattern of central section arrangement. (c) Details of the edge of the metalens.

compared with that of bare LN films. We note that, due to the large intrinsic $\chi^{(2)}$ of the LN material, the SHG efficiency of LN films ($\sim 10^{-5}$ at a pump intensity of 4.05GW/cm^2[47]) is much higher than most nonlinear metamaterial/metasurfaces.[26,28] Hence, our patterned LN films are expected to radiate brighter SHG. Considering that it is difficult to simulate the SHG efficiency of the whole structure, we simulated the SHG efficiency of a single structure to simulate the approximate conversion efficiency, which is detailed in the Supporting Information Note I, Figure S2. We calculated the efficiency of periodic arrays of LN structures and the pure LN film separately at a pumping power density of 4.34×10^8 W/cm^2. The conversion efficiency of periodic arrays of LN structures is 1.4×10^{-4}, and the conversion efficiency of the pure LN film is 2.7×10^{-6} in 780 nm. In our simulation, the simulated SHG efficiency of periodic arrays of LN structures is improved by more than an order of magnitude compared to that of bare LN films. This computation allows us to estimate the simulated metalens' nonlinear conversion efficiency, which will be higher than that of other typical nonlinear metalens. To generate the phase gradient of SHG and create spherical phase distributions for metalens, we deform the circular nanohole into an elliptical nanohole. The major (minor) axis of the elliptical nanohole ranges from 200 to 400 nm. The simulated phases (Figure 1d) and amplitudes (Figure 1e) of the emitted second harmonic waves (wavelength 390 nm) vary continuously (the specific points of phase and amplitude chosen have been marked in the figure using black dots). The second harmonic phase covers the 2π range, which can generate a meta-atom library for nonlinear metalens.

We have selected 25 meta-atom sizes, and their corresponding meta-atom sizes, SHG phases, and amplitudes are shown in Figure 2a. We ensure that the SHG phases of the selected elliptical holes range from $-\pi$ and π, and meanwhile, the amplitudes cover a large value as much as possible. The variations in the SHG amplitudes of the selected nanoholes do not exceed 20%, as shown in Figure 2a. These elliptical nanoholes are arranged according to the phase distribution formula of a spheritic lens:

$$\varphi(r) = \frac{2\pi}{\lambda}(f - \sqrt{r^2 + f^2}) \quad (1)$$

Here, r denotes the distance between the meta-atom's position and the center of the metalens, $f = 100$ μm is the focus length, and $\lambda = 390$ nm is the wavelength of the second harmonic waves. As a result, the phase distribution of every meta-atom is shown in Figure 2b. The diameter of the designed metalens is 200 μm, and thus, the numerical aperture ($N_A = n^* \sin(\theta)$) is $\sim$0.7. The inset images of Figure 2b display enlarged views of the phase profiles, demonstrating that meta-atoms of different sizes can achieve phase coverage from 0 to 2π. For evaluating the performance of the designed nonlinear metalens, we simulate the propagation of the generated second harmonic waves. The optical field μ_0 in the incident plane ($x = 0$, the crystal coordinate systems are employed here where the light propagates along the x-axis) is set according to the SHG phase shown in Figure 2b and the corresponding amplitudes shown in Figure 2a. The propagation of the SHG is then calculated by the Rayleigh–Sommerfeld algorithms. In this way, optical intensity distribution $I(x, y, z)$ in the whole space can be obtained. As shown in Figure 2c, the focal spot fwhm is only 0.68 μm, almost approaching the diffraction limit. The SHG intensity of the brightest point in the focus plane is 220 times stronger than the average intensity of the incident plane, indicating the high-intensity enhancement of SHG. Figure 2d,e show the SHG intensity in the x–y section ($I(x, y, z = 0\ \mu\text{m})$) and in the y–z section at the focus plane ($I(x = f, y, z)$), respectively (for focusing simulations, see Supplementary Note II). These simulation results confirm the focusing ability of the generated second harmonic waves from the LN metalens.

Fabrication of Nonlinear Metalens. The samples of LN films (300 nm thick, x-cut) on the SiO_2 substrate (purchased from Jinan Jingzhen Corporation) are used to fabricate the LN metalens. These films are patterned by using electron beam lithography and inductively coupled plasma enhanced reactive ion etching (ICP-RIE), in which a multiatmosphere cooperative etching technique is proposed for LN nanostructure fabrication (for specific process principles, see Supplementary Note III). This multicomponent atmosphere etching process allows us to obtain LN nanostructures with excellent morphology and a high selectivity ratio (for preparation of LN nonlinear metalens, see Supplementary Note IV). To observe the preparation effect of the nanoholes at different

https://doi.org/10.1021/acsphotonics.4c02259
ACS Photonics XXXX, XXX, XXX−XXX

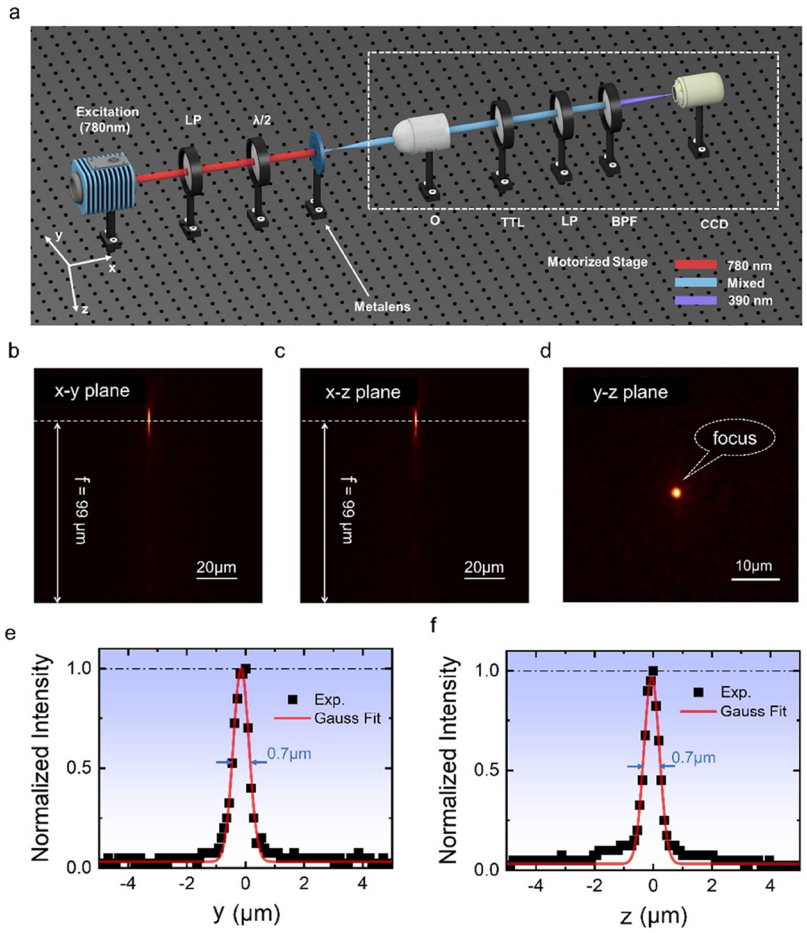

Figure 4. Optical measurement of the second harmonic nonlinear metalens. (a) Experimental setup: $\lambda/2$, half-wave plate; LP, linear polarizer; O, objective; TTL, telescoping telescopic lens; BPF, bandpass filter; CCD, camera; (b,c) Images of the focusing point on different planes: (b) Image of the focusing point on the $x-y$ plane (x = 99 μm); (c) Image of the focusing point on the $x-z$ plane (x = 99 μm). (d) Image of the focusing spot (x = 99 μm). (e,f) Cross sections of the metalens focusing spot, including Gaussian fits in the (e) y-direction and (f) z-direction.

view fields more clearly, we characterized the structural morphology of the LN metalens using an optical microscope (see Supplementary Note V) and SEM (Figure 3a presents a macroscopic picture, exhibiting a clean and residue-free surface of the LN nanohole structure metalens). The diameter of the fabricated metalens is 200 μm. Additionally, in Figure 3b, the metalens clearly exhibits a gradual distribution of LN nanohole sizes and shapes at different phase designs. The edges of the nanoholes are sharp and uniform. Figure 3c shows a magnified close-up of the local morphology at the edge of the metalens, where one can clearly see that the sizes of the LN nanoholes are accurately consistent, with good steepness and smooth side walls, ensuring the metalens' excellent operational efficiency. This guarantees better performance in nonlinear focusing and imaging, enabling more accurate and efficient nonlinear focusing and imaging capabilities. These SEM images demonstrate that we have achieved the processing of LN nanostructure arrays across scales and shapes and that the edges of the nanoholes are sharp and uniform and have high processing precision.

Optical Measurement of the Nonlinear Metalens. The optical measurement systems of the SHG focusing for the fabricated metalens are shown in Figure 4a. The driven light source is a commercial supercontinuous picosecond laser, a spectra range of 450−2400 nm, and a pulse duration of ∼150 ps. The bandpass filter with a central wavelength of 780 nm and a bandwidth of 10 nm is employed to generate the fundamental beam. The power of the incident light is ∼5 mW, and the beam size is ∼2 mm. A polarizer combined with a 1/2 waveplate is used to make the incident light polarize along the optical axis of the LN crystal. After passing through the LN metalens, part of the fundamental light was converted into second harmonic light, while the rest was transmitted through. We employed an objective lens to collect the second harmonic light emitted from the metalens and the transmitted light and then used a linear polarizer to ensure the collected light also polarizes along the optical axis of LN. Subsequently, the SHG and transmitted light pass through a tube lens and a bandpass filter (center wavelength 390 nm and band wavelength 10 nm) and then enter into a camera. In order to scan the intensity distribution of the second harmonic light field at different longitudinal positions, we mounted the objective lens, a second linear polarizer, the bandpass filter, and the CCD camera on a displacement stage controlled by a stepper motor. The integral time constant of the CCD is 1 s.

We utilized the optical testing system described above to test the nonlinear focusing characteristics of the metalens. The measured cross-sectional intensity profiles cross the optic axis in the $x-y$ plane (Figure 4b) and the $x-z$ plane (Figure 4c). The focusing of the SHG light is obviously observed. In both pictures, the vertical distance of the brightest point away from the metalens is 99 μm, which is close to the designed focus

https://doi.org/10.1021/acsphotonics.4c02259
ACS Photonics XXXX, XXX, XXX−XXX

length (100 μm). Figure 4d plots the intensity profile at 99 μm. One can see that the focused spot occupies only a small number of pixels on the CCD (for the three-dimensional focal point image, see Supplementary Note VI). Figure 4e,f displays SHG intensity profiles in the y and z cross sections passing through the focus. By fitting these two curves with the Gaussian function, the half-maximum (fwhm) value of the two intensity profiles is obtained as 0.7 μm, which is in excellent agreement with the theoretical simulation, indicating a good focusing effect. To further evaluate the performance of the metalens, we extracted and analyzed data from its focal plane (see Supporting Information Note VI for the counts figure). This analysis included the focus, the focal plane, and the LN film. The focusing capability of the metalens can be quantified by the intensity enhancement factor, defined as the ratio of the maximum counts (brightest pixel) to the average counts across the focal plane. This factor was measured to be 40, which is five times lower than the simulated results—a discrepancy we attribute to manufacturing imperfections. Additionally, we characterized the SHG emission capabilities of the metalens and compared them to those of the LN film of the same thickness. As illustrated in Figure S8, the LN film exhibits an average SHG integration intensity four times greater than that of the focal plane and one-tenth of that at the focus. Given the inherently high second-order nonlinear coefficient of LN, we conclude that the nonlinear conversion efficiency of the metalens is on the same order of magnitude as that of the intrinsic film. When focusing is taken into account, the efficiency is expected to be 1 order of magnitude higher, significantly exceeding the nonlinear conversion efficiency of the conventional dielectric metalens. These findings demonstrate the successful realization of a nonlinear LN metalens with a high numerical aperture (NA = 0.7) and exceptional second-order nonlinear conversion efficiency. The experimental results align closely with the simulations, underscoring the advanced fabrication capabilities for LN-based devices.

CONCLUSIONS

By combining metasurface photonics with LN nonlinear optics, we have demonstrated that an LN nonlinear metalens not only serves as a compact nonlinear medium for generating second harmonic light but also effectively focuses the produced second harmonic wavefront. The fabricated nonlinear metalens achieves a large numerical aperture of up to 0.7 and a small focal spot of 0.7 μm. Moreover, due to the high second nonlinear susceptibility of LN, we can observe SHG focusing with the excitation of a picosecond supercontinuous laser. At the same time, our metalens has a much higher nonlinear conversion efficiency compared to currently common metalens, and the SHG intensity at the focal point is 10 times higher than that of an LN film of the same thickness and 40 times higher than that of a focal plane. Our metalens exhibits excellent focusing capability, and its numerical aperture can be designed and prepared based on the metalens requirements (see Supplementary Note VII for an LN metalens with N.A. = 0.3 and a diameter of 180 μm). Given the flexibility of the design, more new functionalities can be expected. For example, spontaneous parametric down-conversion (SPDC) metasurfaces can generate entangled photon states. Furthermore, the wavelength affects the lens's image resolutions. Higher resolutions can be achieved with light with shorter wavelengths. Our LN nonlinear metalens with small focal point characteristics thus has broad application prospects in short-wavelength optical imaging.

METHODS

Fabrication. A 100 nm thick layer of Mo mask was deposited onto a 300 nm thick commercially available LN thin film by using a magnetron sputtering device (JSP4). A 500 nm thick layer of e-beam resist (AR-P 6200) was spin-coated onto the Mo mask. After coating, the sample was baked at 150 °C for 1 min. Patterns were exposed using an electron beam lithography system (6300FS, JEOL0) and then developed in a mixture of MIBK and IPA (1:3) for 40 s. It was subsequently rinsed with isopropyl alcohol for 30 s and blow-dried with nitrogen gas. The patterned layer of the AR-P 6200 electron beam resist was used as a mask, and ICP-RIE (Heverlee Pishow A) was used to etch the Mo mask layer for pattern replication and transfer, ultimately obtaining the desired Mo mask pattern. Subsequently, the sample with the Mo mask pattern was placed into an RIE chamber and etched with oxygen to remove any remaining photoresist residue. Finally, the dry etching process was executed in the ICP-RIE system (Plasma lab System 100 ICP180, Oxford) with a mixed reactive gas of Cl_2 to etch the LN. Finally, a scanning electron microscope (Helios 600i, FEI) was used to characterize the morphology of the metalens samples.

Design. The use of COMSOL Multiphysics software allowed for the simulation of both linear and nonlinear properties of the $LiNbO_3$ meta-atoms. The optical constants of $LiNbO_3$ were obtained from ellipsometry measurements, while the refractive index and extinction coefficient of the glass were set for the simulations. In the nonlinear simulation, the specific values for the refractive index and extinction coefficient of the $LiNbO_3$ nanoresonators at the harmonic wavelength were used. Although exact material data for glass at 390 nm was not available, previous research indicated that the effect of the glass substrate and capping layer on the performance of dielectric metasurfaces at the fundamental and harmonic wavelengths was minimal. As a result, the refractive index and extinction coefficient of the glass substrate were set to specific values in the nonlinear simulation in order to streamline the design process (n = 1.45). The absorption of $LiNbO_3$ at 390 nm was found to affect the SHG signal strength but did not shift the resonance position. Periodic boundary conditions were employed in the simulation, and additional details can be found in the Supporting Materials.

ASSOCIATED CONTENT

Data Availability Statement

Statement Research data are not shared.

Supporting Information

The Supporting Information is available free of charge at https://pubs.acs.org/doi/10.1021/acsphotonics.4c02259.

Simulation design of the meta-atom; focusing simulations; preparation of lithium niobate nonlinear metalenses; multiatmosphere combined coetching process; characterization of UV metalens; focusing characterization of the UV metalens; and design, preparation, and testing of the lithium niobate nonlinear metalenses with numerical aperture 0.3 (PDF)

https://doi.org/10.1021/acsphotonics.4c02259
ACS Photonics XXXX, XXX, XXX−XXX

AUTHOR INFORMATION

Corresponding Authors

Bo Wang − *Beijing National Laboratory for Condensed Matter Physics, Institute of Physics, Chinese Academy of Sciences, Beijing 100190, China;* orcid.org/0000-0002-3988-5032; Email: wangbo2014@iphy.ac.cn

Ruhao Pan − *Beijing National Laboratory for Condensed Matter Physics, Institute of Physics, Chinese Academy of Sciences, Beijing 100190, China;* orcid.org/0000-0002-5573-2992; Email: panruhao@iphy.ac.cn

Junjie Li − *Beijing National Laboratory for Condensed Matter Physics, Institute of Physics, Chinese Academy of Sciences, Beijing 100190, China; CAS Key Laboratory of Vacuum Physics, University of Chinese Academy of Sciences, Beijing 100049, China;* orcid.org/0000-0002-1508-9891; Email: jjli@iphy.ac.cn

Authors

Yunan Liu − *Beijing National Laboratory for Condensed Matter Physics, Institute of Physics, Chinese Academy of Sciences, Beijing 100190, China; CAS Key Laboratory of Vacuum Physics, University of Chinese Academy of Sciences, Beijing 100049, China;* orcid.org/0009-0005-9139-327X

Leyong Hu − *Beijing National Laboratory for Condensed Matter Physics, Institute of Physics, Chinese Academy of Sciences, Beijing 100190, China*

Xu Ji − *Beijing National Laboratory for Condensed Matter Physics, Institute of Physics, Chinese Academy of Sciences, Beijing 100190, China*

Tingyue Zhu − *Beijing National Laboratory for Condensed Matter Physics, Institute of Physics, Chinese Academy of Sciences, Beijing 100190, China*

Haifang Yang − *Beijing National Laboratory for Condensed Matter Physics, Institute of Physics, Chinese Academy of Sciences, Beijing 100190, China*

Changzhi Gu − *Beijing National Laboratory for Condensed Matter Physics, Institute of Physics, Chinese Academy of Sciences, Beijing 100190, China; CAS Key Laboratory of Vacuum Physics, University of Chinese Academy of Sciences, Beijing 100049, China;* orcid.org/0000-0002-2689-2807

Complete contact information is available at: https://pubs.acs.org/10.1021/acsphotonics.4c02259

Funding

This work was supported by the National Natural Science Foundation of China (Grant Nos. 12074420, U21A20140, 61888102, 12204527, and 61905274), the Beijing Municipal Science & Technology Commission, Administrative Commission of Zhongguancun Science Park (No. Z211100004821009), the Chinese Academy of Sciences through the Project for Young Scientists in Basic Research (YSBR-021), and the Key Research Program of Frontier Sciences of Chinese Academy of Sciences (Grant No. QYZDJ-SSWSLH042 and XDPB22). This work was also supported by the Synergic Extreme Condition User Facility, China (SECUF, https://cstr.cn/31123.02.SECUF).

Notes

The authors declare no competing financial interest.

REFERENCES

(1) Li, C.; Du, S.; Pan, R.; Xiong, X.; Tang, Z.; Zheng, R.; Liu, Y.; Geng, G.; Sun, J.; Gu, C.; et al. Phase Change Materials-Based Bilayer Metasurfaces for Near-Infrared Photonic Routing. *Adv. Funct. Mater.* **2023**, *34*, No. 2310626.

(2) Cai, G.; Li, Y.; Zhang, Y.; Jiang, X.; Chen, Y.; Qu, G.; Zhang, X.; Xiao, S.; Han, J.; Yu, S.; et al. Compact angle-resolved metasurface spectrometer. *Nat. Mater.* **2024**, *23*, 71−78.

(3) Cheng, Y.; Zhou, C.; Yuan, B. G.; Wu, D. J.; Wei, Q.; Liu, X. J. Ultra-sparse metasurface for high reflection of low-frequency sound based on artificial Mie resonances. *Nat. Mater.* **2015**, *14*, 1013−1019.

(4) Almeida, E.; Shalem, G.; Prior, Y. Subwavelength nonlinear phase control and anomalous phase matching in plasmonic metasurfaces. *Nat. Commun.* **2016**, *7*, 10367.

(5) Chen, H. T.; Taylor, A. J.; Yu, N. A review of metasurfaces: physics and applications. *Rep. Prog. Phys.* **2016**, *79*, No. 076401.

(6) Dong, T.; Li, S.; Manjappa, M.; Yang, P.; Zhou, J.; Kong, D.; Quan, B.; Chen, X.; Ouyang, C.; Dai, F.; et al. Nonlinear THz-Nano Metasurfaces. *Adv. Funct. Mater.* **2021**, *31*, No. 2100463.

(7) Pan, M.; Fu, Y.; Zheng, M.; Chen, H.; Zang, Y.; Duan, H.; Li, Q.; Qiu, M.; Hu, Y. Dielectric metalens for miniaturized imaging systems: progress and challenges. *Light: Sci. Appl.* **2022**, *11*, 195.

(8) Zhao, M.; Chen, M. K.; Zhuang, Z. P.; Zhang, Y.; Chen, A.; Chen, Q.; Liu, W.; Wang, J.; Chen, Z. M.; Wang, B.; et al. Phase characterisation of metalenses. *Light: Sci. Appl.* **2021**, *10*, 52.

(9) Lim, S. W. D.; Meretska, M. L.; Capasso, F. A High Aspect Ratio Inverse-Designed Holey metalens. *Nano Lett.* **2021**, *21*, 8642−8649.

(10) Park, J. S.; Zhang, S.; She, A.; Chen, W. T.; Lin, P.; Yousef, K. M. A.; Cheng, J. X.; Capasso, F. All-Glass, Large metalens at Visible Wavelength Using Deep-Ultraviolet Projection Lithography. *Nano Lett.* **2019**, *19*, 8673−8682.

(11) Chen, W. T.; Zhu, A. Y.; Sisler, J.; Bharwani, Z.; Capasso, F. A broadband achromatic polarization-insensitive metalens consisting of anisotropic nanostructures. *Nat. Commun.* **2019**, *10*, 355.

(12) Fan, Z. B.; Qiu, H. Y.; Zhang, H. L.; Pang, X. N.; Zhou, L. D.; Liu, L.; Ren, H.; Wang, Q. H.; Dong, J. W. A broadband achromatic metalens array for integral imaging in the visible. *Light: Sci. Appl.* **2019**, *8*, 67.

(13) Lin, R. J.; Su, V. C.; Wang, S.; Chen, M. K.; Chung, T. L.; Chen, Y. H.; Kuo, H. Y.; Chen, J. W.; Chen, J.; Huang, Y. T.; et al. Achromatic metalens array for full-colour light-field imaging. *Nat. Nanotechnol.* **2019**, *14*, 227−231.

(14) Lee, G. Y.; Hong, J. Y.; Hwang, S.; Moon, S.; Kang, H.; Jeon, S.; Kim, H.; Jeong, J. H.; Lee, B. Metasurface eyepiece for augmented reality. *Nat. Commun.* **2018**, *9*, 4562.

(15) Malek, S. C.; Overvig, A. C.; Alù, A.; Yu, N. Multifunctional resonant wavefront-shaping meta-optics based on multilayer and multi-perturbation nonlocal metasurfaces. *Light: Sci. Appl.* **2022**, *11*, 246.

(16) Jin, C.; Afsharnia, M.; Berlich, R.; Fasold, S.; Zou, C.; Arslan, D.; Staude, I.; Pertsch, T.; Setzpfandt, F. Dielectric metasurfaces for distance measurements and three-dimensional imaging. *Adv. Photonics* **2019**, *1*, No. 036001.

(17) Chen, B. H.; Wu, P. C.; Su, V. C.; Lai, Y. C.; Chu, C. H.; Lee, I. C.; Chen, J. W.; Chen, Y. H.; Lan, Y. C.; Kuan, C. H.; et al. GaN metalens for Pixel-Level Full-Color Routing at Visible Light. *Nano Lett.* **2017**, *17*, 6345−6352.

(18) Miyata, M.; Nakajima, M.; Hashimoto, T. High-Sensitivity Color Imaging Using Pixel-Scale Color Splitters Based on Dielectric Metasurfaces. *ACS Photonics* **2019**, *6*, 1442−1450.

(19) Zheng, R.; Pan, R.; Geng, G.; Jiang, Q.; Du, S.; Huang, L.; Gu, C.; Li, J. Active multiband varifocal metalenses based on orbital angular momentum division multiplexing. *Nat. Commun.* **2022**, *13*, 4292.

(20) Tymchenko, M.; Gomez Diaz, J. S.; Lee, J.; Nookala, N.; Belkin, M. A.; Alù, A. Gradient Nonlinear Pancharatnam-Berry Metasurfaces. *Phys. Rev. Lett.* **2015**, *115*, No. 207403.

(21) Lemoult, F.; Lerosey, G.; de Rosny, J.; Fink, M. Resonant Metalenses for Breaking the Diffraction Barrier. *Phys. Rev. Lett.* **2010**, *104*, No. 203901.
(22) Zhou, H. P.; Chen, L.; Shen, F.; Guo, K.; Guo, Z. Y. Broadband Achromatic metalens in the Midinfrared Range. *Phys. Rev. Appl.* **2019**, *11*, No. 024066.
(23) Xie, R. S.; Zhai, G. H.; Wang, X.; Zhang, D. J.; Si, L. M.; Zhang, H. L.; Ding, J. High-Efficiency Ultrathin Dual-Wavelength Pancharatnam-Berry Metasurfaces with Complete Independent Phase Control. *Adv. Opt. Mater.* **2019**, *7*, No. 1900594.
(24) Ding, X. M.; Monticone, F.; Zhang, K.; Zhang, L.; Gao, D. L.; Burokur, S. N.; de Lustrac, A.; Wu, Q.; Qiu, C. W.; Alu, A. Ultrathin Pancharatnam-Berry Metasurface with Maximal Cross-Polarization Efficiency. *Adv. Mater.* **2015**, *27*, 1195−1200.
(25) Zhou, J. X.; Zhao, J. X.; Wu, Q. Y.; Chen, C. F.; Lei, M.; Chen, G. H.; Tian, F. L.; Liu, Z. W. Nonlinear Computational Edge Detection metalens. *Adv. Funct. Mater.* **2022**, *32*, No. 2204734.
(26) Tseng, M. L.; Semmlinger, M.; Zhang, M.; Arndt, C.; Huang, T. T.; Yang, J.; Kuo, H. Y.; Su, V. C.; Chen, M. K.; Chu, C. H.; et al. Vacuum ultraviolet nonlinear metalens. *Sci. Adv.* **2022**, *8*, No. eabn5644.
(27) Ossiander, M.; Meretska, M. L.; Hampel, H. K.; Lim, S. W. D.; Knefz, N.; Jauk, T.; Capasso, F.; Schultze, M. Extreme ultraviolet metalens by vacuum guiding. *Science* **2023**, *380*, 59−63.
(28) Schlickriede, C.; Waterman, N.; Reineke, B.; Georgi, P.; Li, G. X.; Zhang, S.; Zentgraf, T. Imaging through Nonlinear metalens Using Second Harmonic Generation. *Adv. Mater.* **2018**, *30*, No. 1703843.
(29) Zhu, D.; Shao, L. B.; Yu, M. J.; Cheng, R.; Desiatov, B.; Xin, C. J.; Hu, Y. W.; Holzgrafe, J.; Ghosh, S.; Shams Ansari, A.; et al. Integrated photonics on thin-film lithium niobate. *Adv. Opt. Photonics* **2021**, *13*, 242−352.
(30) Qi, Y.; Li, Y. Integrated lithium niobate photonics. *Nanophotonics* **2020**, *9*, 1287−1320.
(31) Kim, K. H.; Rim, W. S. Anapole Resonances Facilitated by High-Index Contrast between Substrate and Dielectric Nanodisk Enhance Vacuum Ultraviolet Generation. *ACS Photonics* **2018**, *5*, 4769−4775.
(32) Snigirev, V.; Riedhauser, A.; Lihachev, G.; Churaev, M.; Riemensberger, J.; Wang, R. N.; Siddharth, A.; Huang, G.; Möhl, C.; Popoff, Y.; et al. Ultrafast tunable lasers using lithium niobate integrated photonics. *Nature* **2023**, *615*, 411−417.
(33) Weis, R. S.; Gaylord, T. K. Lithium niobate: Summary of physical properties and crystal structure. *Appl. Phys. A: Mater. Sci. Process.* **1985**, *37*, 191−203.
(34) Qu, L.; Bai, L.; Jin, C.; Liu, Q.; Wu, W.; Gao, B.; Li, J.; Cai, W.; Ren, M.; Xu, J. Giant Second Harmonic Generation from Membrane Metasurfaces. *Nano Lett.* **2022**, *22*, 9652−9657.
(35) Ma, J.; Xie, F.; Chen, W.; Chen, J.; Wu, W.; Liu, W.; Chen, Y.; Cai, W.; Ren, M.; Xu, J. Nonlinear Lithium Niobate Metasurfaces for Second Harmonic Generation. *Laser Photonics Rev.* **2021**, *15*, No. 2000521.
(36) Fedotova, A.; Younesi, M.; Sautter, J.; Vaskin, A.; Löchner, F. J. F.; Steinert, M.; Geiss, R.; Pertsch, T.; Staude, I.; Setzpfandt, F. Second Harmonic Generation in Resonant Nonlinear Metasurfaces Based on Lithium Niobate. *Nano Lett.* **2020**, *20*, 8608−8614.
(37) Carletti, L.; Zilli, A.; Moia, F.; Toma, A.; Finazzi, M.; De Angelis, C.; Neshev, D. N.; Celebrano, M. Steering and Encoding the Polarization of the Second Harmonic in the Visible with a Monolithic LiNbO3Metasurface. *ACS Photonics* **2021**, *8*, 731−737.
(38) Weigand, H.; Vogler Neuling, V. V.; Escalé, M. R.; Pohl, D.; Richter, F. U.; Karvounis, A.; Timpu, F.; Grange, R. Enhanced Electro-Optic Modulation in Resonant Metasurfaces of Lithium Niobate. *Acs Photonics* **2021**, *8*, 3004−3009.
(39) Timpu, F.; Weigand, H.; Kaufmann, F.; Richter, F. U.; Vogler-Neuling, V. V.; Karvounis, A.; Grange, R. Towards active electro-optic lithium niobate metasurfaces. *EPJ Web Conf.* **2020**, *238*, No. 05003.
(40) Zhang, J. H.; Ma, J. Y.; Parry, M.; Cai, M.; Camacho Morales, R.; Xu, L.; Neshev, D. N.; Sukhorukov, A. A. Spatially entangled photon pairs from lithium niobate nonlocal metasurfaces. *Sci. Adv.* **2022**, *8*, No. eabq4240.
(41) Zhao, J.; Ma, C.; Rüsing, M.; Mookherjea, S. High Quality Entangled Photon Pair Generation in Periodically Poled Thin-Film Lithium Niobate Waveguides. *Phys. Rev. Lett.* **2020**, *124*, No. 163603.
(42) Pohl, D.; Escalé, M. R.; Madi, M.; Kaufmann, F.; Brotzer, P.; Sergeyev, A.; Guldimann, B.; Giaccari, P.; Alberti, E.; Meier, U.; et al. An integrated broadband spectrometer on thin-film lithium niobate. *Nat. Photonics* **2020**, *14*, 24−29.
(43) Li, M.; Ling, J.; He, Y.; Javid, U. A.; Xue, S.; Lin, Q. Lithium niobate photonic-crystal electro-optic modulator. *Nat. Commun.* **2020**, *11*, 4123.
(44) Zhang, M.; Buscaino, B.; Wang, C.; Shams Ansari, A.; Reimer, C.; Zhu, R.; Kahn, J. M.; Lončar, M. Broadband electro-optic frequency comb generation in a lithium niobate microring resonator. *Nature* **2019**, *568*, 373−377.
(45) Wang, C.; Zhang, M.; Yu, M. J.; Zhu, R. R.; Hu, H.; Loncar, M. Monolithic lithium niobate photonic circuits for Kerr frequency comb generation and modulation. *Nat. Commun.* **2019**, *10*, 978.
(46) Wang, C.; Li, Z. Y.; Kim, M. H.; Xiong, X.; Ren, X. F.; Guo, G. C.; Yu, N. F.; Loncar, M. Metasurface-assisted phase-matching-free second harmonic generation in lithium niobate waveguides. *Nat. Commun.* **2017**, *8*, 2098.
(47) Ma, J. J.; Chen, J. X.; Ren, M. X.; Wu, W.; Cai, W.; Xu, J. J. Second-harmonic generation and its nonlinear depolarization from lithium niobate thin films. *Opt. Lett.* **2020**, *45*, 145−148.

https://doi.org/10.1021/acsphotonics.4c02259
ACS Photonics XXXX, XXX, XXX−XXX